Mechanics of Materials 195 (2024) 105027

Contents lists available at ScienceDirect

Mechanics of Materials

journal homepage: www.elsevier.com/locate/mechmat

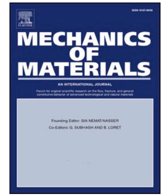

Research paper

Concurrent delamination propagation and deformation localization in semiconductor devices

Shawn R. Lavoie[a], Guodong Nian[a], Chen-Wei Li[b], Jason Lan[b], Yu-Sheng Lin[b], Yi-Lun Lin[b], Sherwin Tang[b], Jyun-Lin Wu[b], Joost J. Vlassak[a], Zhigang Suo[a,*]

[a] *John A. Paulson School of Engineering and Applied Sciences, Harvard University, Cambridge, MA, 02138, USA*
[b] *Quality and Reliability, Taiwan Semiconductor Manufacturing Company, Ltd., Hsinchu, Taiwan, ROC*

ARTICLE INFO

Keywords:
Delamination
Necking
Metal
Polymer
Semiconductor devices

ABSTRACT

In semiconductor devices, metals and polymers are often integrated as electrical conductors and insulators. Fabrication and operation of the devices cause stress in such an integrated structure. The stress can delaminate the metals and polymers, as well as deform them plastically. Here we show that the delamination can localize the deformation in the metals, which form necks to rupture the metals and sever electrical conduction. We simulate the coevolution of delamination propagation and deformation localization. The metals and polymers are modeled as elastic-plastic materials, and their adhesion is represented by a cohesive zone model. The simulation highlights that extensive delamination is a prerequisite for the metals to form necks, and that necking causes delamination to propagate further. Also highlighted are the impact of corners in the structure. Preexisting defects make the structure particularly vulnerable to concurrent delamination and necking. It is hoped that this study will draw renewed attention to the mechanical behavior of materials in the development of the semiconductor industry.

1. Introduction

Semiconductor manufacturing is undergoing rapid development, driven by ABCDE applications, short for artificial intelligence, blockchain, cloud computing, data, and energy-efficient phones (Lau, 2022). In addition to miniaturizing features on an individual chip, a potent approach is to stack many chips on a substrate, an architecture called three-dimensional integrated circuits (3D ICs). This architecture reduces connection lengths, lowers power consumption, shortens signal propagation time, and makes designs compact.

In a representative 3D IC, multiple chips are stacked on a single substrate. To focus attention to a specific phenomenon, consider one chip on a substrate (Fig. 1a). The chip, diced from a wafer, consists of dissimilar materials integrated by wafer processing. The substrate is a composite of metals and polymers. On the surface of the chip are electroplated solder bumps. The chip and the substrate are placed in contact, and the solder bumps are fused to metals on the substrate at an elevated temperature. The chip has a smaller coefficient of thermal expansion (CTE) than the substrate. Upon a change in temperature, this mismatch in CTE causes stress, which concentrates at the edge of the chip.

This paper focuses on a failure mechanism in an integrated structure of metal and polymer (Fig. 1b). During fabrication and operation, the stress in the devices may cause the metals and polymers to delaminate and deform. If the metal delaminates from the polymer, the debonded metal is vulnerable to localized deformation, namely, necking. The necking may rupture the metals and sever electrical conduction. By contrast, if the metal and the polymer are bonded, the deformation in the metal will not localize, so that even a large deformation will not sever the metal and cause electrical failure.

The failure mechanism described here involves two well-known phenomena: localization of deformation and propagation of delamination. Professor Alan Needelman has made seminal contributions to the understanding of both phenomena. In the early 1970s, when large elastic-plastic deformation began to be amenable to finite element analysis, he published a paper, entitled, “A Numerical Study of Necking in Circular Cylindrical Bar” (Needleman, 1972). When a metal bar is pulled, the deformation is homogeneous when the strain is small, and then a neck sets in when the strain exceeds a critical value. The inhomogeneous, localized deformation can be fully captured by the finite element analysis until the bar ruptures. Even though necking of metals

* Corresponding author.
E-mail address: suo@seas.harvard.edu (Z. Suo).

https://doi.org/10.1016/j.mechmat.2024.105027
Received 1 March 2024; Received in revised form 1 May 2024; Accepted 2 May 2024
Available online 4 May 2024
0167-6636/© 2024 Elsevier Ltd. All rights reserved.

had been well-known to engineers, a finite element analysis enabled the phenomenon to be studied numerically, so that the significance of various parameters could be examined.

In the 1980s, the development of composite materials caught the imagination of the community of mechanics and materials. In particular, a class of composites involved metallic matrices and ceramic particles. When such a composite is loaded, the metallic matrix undergoes large plastic deformation, and the ceramic particles undergo small elastic deformation. This difference in types of deformation often debonds the metallic matrix and ceramic particles. Because the plastic zone is comparable to the feature size of the composite, the elastic fracture mechanics does not apply. Professor Alan Needleman met this challenge by publishing the paper, entitled, "A Continuum Model for Void Nucleation by Inclusion Debonding" (Needleman, 1987). He represented the adhesion between the metallic matrix and ceramic particles by a traction-displacement relation, also called a crack bridging model, or cohesive zone model. Although such a cohesive zone model had been previously introduced (Barenblatt, 1959; Dugdale, 1960), the model had been used by compiling the traction-displacement curve to linear elastic materials. The paper by Professor Alan Needleman recognized the significance of the concurrent plastic deformation and interfacial debonding.

Here we show the lessons taught in the two seminal papers of Alan Needleman are essential to the understanding of a failure mechanism in semiconductor devices. A 3D IC involves dissimilar materials and complex geometries. The complexity complicates failure analysis. Specifically, both delamination and deformation are progressive and concurrent. It is unrealistic to prescribe a fixed area of delamination and simulate the deformation alone. Specifically, as noted above, we focus on a failure mechanism involving concurrent delamination propagation and deformation localization. The two processes facilitate each other. If delamination does not propagate, deformation will not localize. If deformation does not localize, delamination will not propagate. Following Needleman (1987), we represent the metal and the polymer as elastic-plastic materials (Fig. 1c and d), and represent their adhesion by a traction-displacement curve (Fig. 1e). We specify the model in detail (Section 2). To gain insight into concurrent delamination propagation and deformation localization, we analyze a relatively simple structure: a thin metal layer sandwiched between two polymer blocks (Section 3). To highlight issues arising from the complexity of an integrated structure, we consider a structure in which a metal layer forms a corner (Section 4). We hope that this paper will bring the lessons taught by Professor Alan Needleman to engineers in the development of the semiconductor industry.

2. Methods

Concurrent deformation and delamination have become important themes in mechanics of materials since the pioneering works by Needleman. By following the approach demonstrated by him, many phenomena have been studied. Examples include voids growth (Tvergaard, 1990), necking (Li and Suo, 2007), fracture of ductile metals (Tvergaard and Hutchinson, 1992), fracture of polymer networks (Hui et al., 2003; Zhang et al., 2017), and debonding of metal films from substrates (Wei and Hutchinson, 1997). Here we adopt Needleman's approach to analyze integrated metal-polymer structures in semiconductor devices.

The metal and the polymer are modeled as elastic-plastic materials, with the uniaxial tensile stress-strain curve given by (Fig. 1c and d)

$$\sigma = \begin{cases} E\varepsilon, & \varepsilon \le \dfrac{\sigma_Y}{E} \\ \sigma_Y\left(\dfrac{E\varepsilon}{\sigma_Y}\right)^N, & \varepsilon > \dfrac{\sigma_Y}{E} \end{cases} \tag{1}$$

where σ is the true stress, ε is the natural strain, E is modulus, and N is the strain-hardening exponent. Our simulations assume specific values for various parameters (Table 1). In multiaxial stress states, upon loading and unloading, the metal and the polymer are modeled by the J_2 flow theory.

Table 1
Material parameters for metal and polymer.

Material	E (GPa)	N	σ_Y (MPa)	CTE
Metal	120	0.12	165	1.7×10^{-5}
Polymer	3.3	0.1	125	1.0×10^{-3}

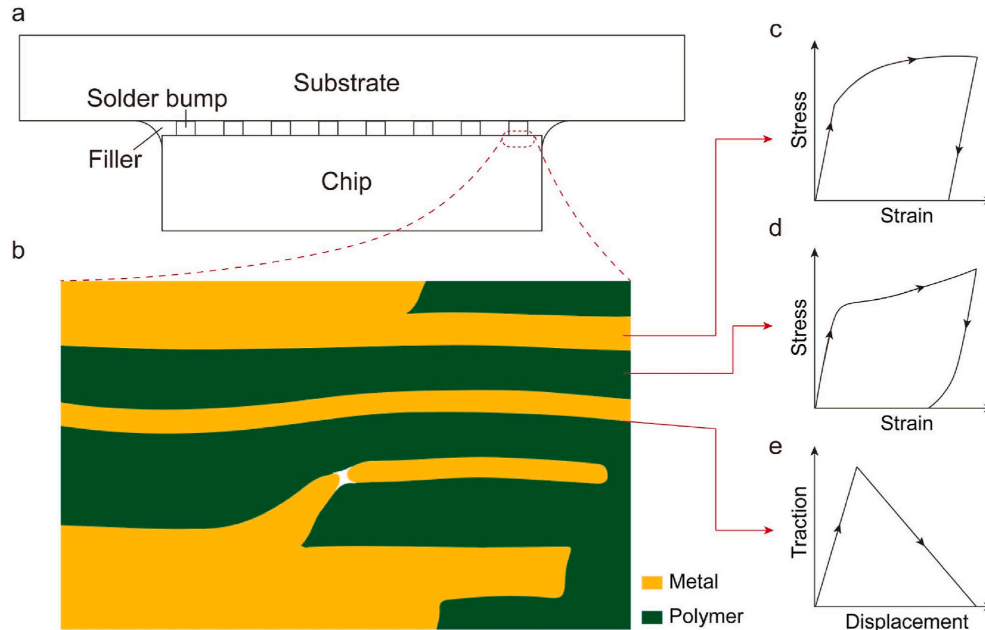

Fig. 1. Failure in an integrated structure of metal and polymer. (a) Schematic of a chip on a substrate. (b) Near the edge of the chip, a region contains metal layers embedded in a polymer. The structure undergoes concurrent delamination and necking. Stress-strain curves of (c) the metal, and (d) the polymer. (e) Traction-displacement relation of the interface.

The integrated structure is assumed to deform under plane-strain conditions. The crack tip concentrates stress, so that the metal and the polymer yield within a plastic zone. To advance the crack, the two materials must deform in their volumes and separate along their interface. When the plastic zone size is much smaller than the feature size of a body, the plastic zone size is a material property, so that the resistance to interfacial debond is characterized by a material property, toughness. This case is called small-scale yielding. When the plastic zone is comparable to the feature size of the body, the resistance to interfacial debond is not a material property. This case is called large-scale yielding. Under the small-scale yielding condition, the plastic zone size is estimated by (Irwin, 1968)

$$r_p = \frac{G_c E}{2\pi {\sigma_Y}^2} \tag{2}$$

where G_c is the toughness, E is the modulus, and σ_Y is the yield strength. This formula can be used to estimate the plastic zone in either material, with the yield strength of that material. The modulus is determined by $E = 1/(1/E_{metal}+1/E_{polymer}) \sim 3$ GPa (Malyshev and Salganik, 1965). In our example, the yield strength of the polymer is smaller than that of the metal. Thus, the plastic zone in the polymer is larger than that in the metal. We will use the plastic zone in the polymer to represent the extent of the plastic zone. To estimate, we assume an interfacial toughness of $G_c \sim 10$ J/m^2, and use a yield strength of the polymer of $\sigma_Y \sim 100$ MPa, so that the plastic zone size is $r_p \sim 0.5$ μm. The plastic zone size is comparable to the feature size in the integrated structure (~1 μm), indicating that large-scale yielding prevails. Consequently, for semiconductor devices, we usually cannot use a material property, toughness, to characterize fracture resistance. That is, linear elastic fracture mechanics usually does not apply to the integrated structures of metals and polymers in semiconductor devices.

In our simulations, the cohesive zone model (CZM) is used to represent the adhesion between the metal and polymer. The interface can both open and slide. For both opening and sliding modes, we adopt the bilinear CZM, which consists of two lines (Fig. 1e). For both modes, we assume the slope of the first line is 1.0×10^8 N/mm^3. Such a high value represents a stiff response of the interface prior to damage. There seems no basis for specifying a value of the stiffness. However, numerical results are often not sensitive to the choice of the stiffness (Needleman, 1987). We adopt the quadratic nominal stress criterion:

$$\left(\frac{\langle \sigma_n \rangle}{N_{max}}\right)^2 + \left(\frac{\sigma_s}{S_{max}}\right)^2 = 1 \tag{3}$$

where σ_n, and σ_s are normal and shear stresses, respectively, N_{max} and S_{max} are critical normal and shear stress, respectively, and the operator '< >' sets negative values to zero. When condition (3) is reached, the stress starts to go down along the second line. We represent a weak interface by $N_{max} = 150$ MPa and $S_{max} = 175$ MPa. We represent a strong interface by $N_{max} = 550$ MPa and $S_{max} = 625$ MPa. For both opening and sliding mode, we specify that the stresses vanish when the displacement reaches 6.7×10^{-8} m. These parameters correspond to a range of toughness of $G_c = 5$–21 J/m^2. Note that in the bilinear CZM, the traction-displacement curve and the horizontal axis form a triangle (Fig. 1e), in which the height corresponds to the critical stress, the length of the base corresponds to the critical displacement, and the area corresponds to the toughness.

3. Concurrent delamination and deformation of a metal film sandwiched between two polymer substrates

Rupture of a metal by localized deformation is well known. For example, consider a metal wire, its length being much larger than its diameter. When pulled, the wire deforms homogeneously when the strain is small, and then forms a neck. The critical strain for the onset of necking is set by the hardening exponent of the metal. For a metal of negligible strain hardening, the critical strain is small, say 1%. Once the neck sets in, further deformation localizes in the neck, while the remaining long metal wire unloads. The neck takes place in a segment in the wire, with length of the segment being comparable to the diameter of the wire. Even though the strain in the neck is large, say, over 100%, the strain in the rest of the wire is small. The long wire snaps to rupture, like a piano wire.

Next consider a thin metal film on a polymer substrate (Li et al., 2004, 2005; Li and Suo, 2007; Lu et al., 2007, 2009). The metal-polymer laminate is pulled in tension. If the metal and the polymer are bonded, the presence of the polymer suppresses strain localization in the metal, and the metal deforms homogeneously to a large strain without rupture. If the metal and the polymer debond, the debonded metal behaves similarly to a metal wire, which forms a neck and ruptures at a small strain. The propagation of delamination and localization of deformation are concurrent and facilitate each other (Li and Suo, 2007).

The integrated structure in a semiconductor device is complex, which masks the basic mechanics of concurrent delamination propagation and deformation localization. To illustrate an aspect of this complexity, this section considers an idealized integrated structure in which two layers of polymer sandwich a layer of metal. If the metal is well bonded to the polymer, metal and polymer deform concurrently (Fig. 2a). The deformation is homogeneous in each layer. If the metal delaminates from the polymer, the debonded metal is vulnerable to localized deformation (Fig. 2b). The localized deformation causes stresses to concentrate at the fronts of the delamination, which facilitates delamination propagation. The localization of deformation and propagation of the delamination facilitate each other. They coevolve.

The delamination is a prerequisite for the deformation localization. This prerequisite has been studied by previous works focused on a thin metal film on a thick polymer substrate (Li and Suo, 2007; Lu et al., 2007). For the film/substrate structure, the metal is only confined by the polymer on one side, while the other side is free of any confinement. By contrast, in the sandwich structure, the metal is confined by the polymer on both sides. Consequently, delamination on one side of the metal may not cause localized deformation, as the other side of the metal is still confined by the polymer. As an illustration, we introduce a debond on one interface, and then pull the sandwich (Fig. 3). The deformation in each layer remains homogeneous. Because the displacement applied in the horizontal direction generates no traction on the interface, the delamination does not propagate. In this figure the metal is shown in orange, and the polymer substrates are shown in green. The cohesive elements are too thin to be visible.

As a second example, we introduce a wedge-like flaw on one

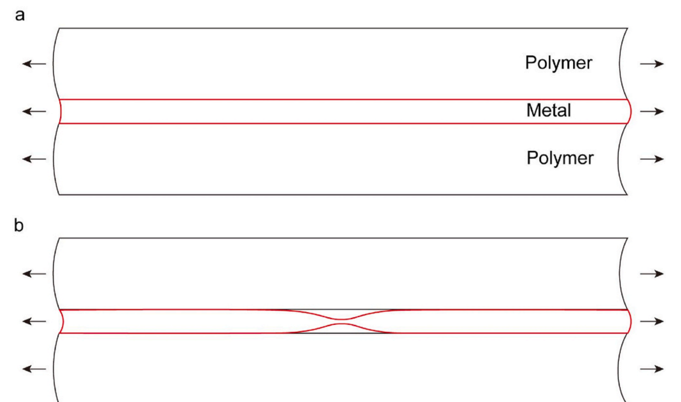

Fig. 2. A tensile displacement is applied to a metal film sandwiched between two polymer substrates. The adhesion is represented by cohesive elements. (a) When the film and the substrate do not debond, the film deforms homogeneously. (b) When the film debonds from both substrates, the deformation of the film localizes into a neck.

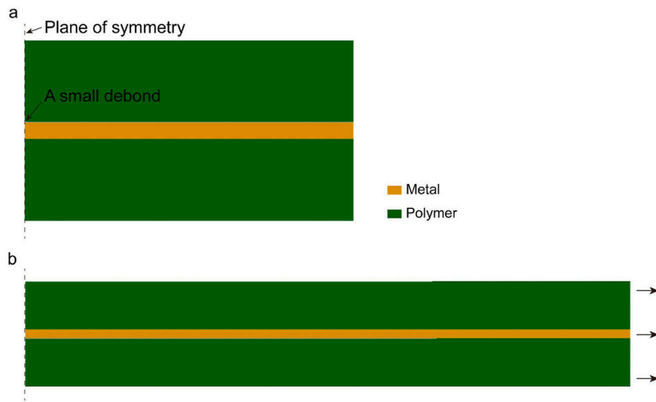

Fig. 3. (a) In the undeformed state, one interface is introduced with a small debond, but the other interface remains bonded. (b) When the laminate is pulled by an applied displacement, the metal film deforms homogeneously. The metal film, the polymer substrate, and the interface are shown in orange, green, and gray, respectively.

interface, and then pull the sandwich (Fig. 4). In the finite element model, the flaw is a region where materials are removed and the mesh around the flaw is refined. The deformation in the metal is no longer homogeneous, and some traction is generated on the interface. The traction may be high enough to cause further debonding. Furthermore, the inhomogeneous deformation also causes transverse stress in the metal, which may cause the other interface to debond. The combined effect can localize the deformation in the metal into a neck. The amount of pulling to cause the deformation in the metal to localize depends on the various material properties, as well as the properties of the cohesive elements. Specifically, with the properties of the metal and polymer fixed, strong adhesion between the two materials will retard the localization of the deformation in the metal.

As a third example, consider the effect of a stress applied normal to the interfaces (Fig. 5). In an integrated structure in a semiconductor device, such a transverse tensile stress commonly arises due to misfit in the coefficients of thermal expansion of the metal and polymer. The transverse stress encourages debonding, which in turn encourages the metal to localize deformation. Here we take the model from Fig. 4 and apply a small tensile stress (50 MPa) normal to the top and bottom surfaces of the structure. This transverse stress in combination with the longitudinal tensile displacement, causes the metal to debond from both

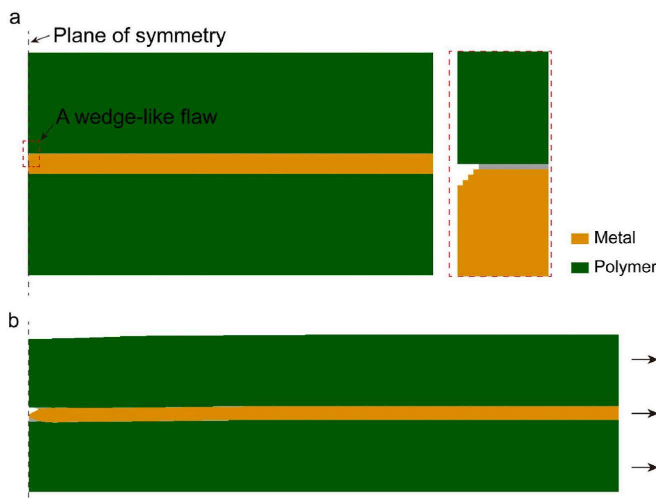

Fig. 4. (a) In the reference state, a wedge-like flaw is introduced at one interface, but the other interface is bonded. (b) When the laminate is pulled, the other interface debonds, which leads to the necking of the metal film.

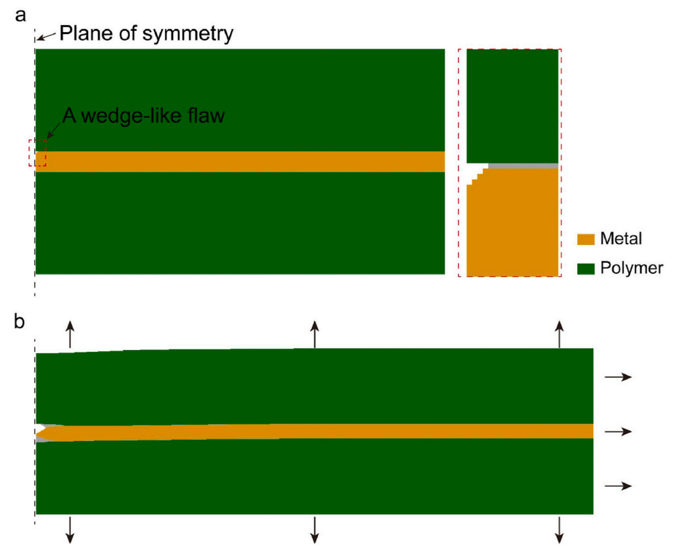

Fig. 5. A transverse tensile stress will promote debond, and reduce the longitudinal stretch at which the metal forms a neck.

polymer substrates, facilitating deformation localization at a lower strain than that in Fig. 4.

4. Concurrent delamination and deformation in an integrated structure

To further illustrate concurrent propagation of delamination and localization of deformation, we revisit the integrated structure in a semiconductor device described in the introduction (Fig. 1). We represent a part of the structure using a finite element model (Fig. 6a). Since failure is observed to concentrate at the bend of the metal layer (Fig. 1b), we introduce a small preexisting delamination at the corner of the bottom surface of the metal layer and use cohesive elements on both sides of the metal layer in this area.

We displace the block in shear by the following boundary conditions. Displacements in the horizontal directions are applied on the left and right edges. Displacements vary from 0 at the bottom edge to 0.0037 mm at the top edge. The displacements are varied cubically to give higher shear stress on the top surface of the metal layer than the bottom. Displacements in the vertical direction are held fixed on all four edges. These displacements are applied using a DISP subroutine in the software ABAQUS. The metal and the polymer are given different coefficients of thermal expansion (Table 1). Simultaneous to the increase of the displacement, the temperature is ramped to decrease by 20 °C. This is a smaller temperature decrease than the device experiences. In our calculation we model only a small part of a full device and prescribe displacements on the boundaries, so that the boundaries have no compliance, and a large change in temperature will result in extensive delamination of the structure. By contrast, in the actual device there is significant compliance of the surrounding structure, so that a change in temperature will not cause as much stress on the metal/polymer interface.

The applied displacement shears the polymer relative to the metal, whereas the change in temperature can cause a complex stress field. In particular, stress components acting on the interface can also promote delamination. Note that the metal layer is bent around the corner, where the metal/polymer interface is not parallel to the top and bottom surfaces of our model. The shear displacement applied on the boundaries of our model causes compression on the inclined part of the metal/polymer interface. This compression suppresses the opening of the interface. Recall that a tension promotes the opening of the interface (Fig. 5). Without applying a change in temperature, it is difficult for our

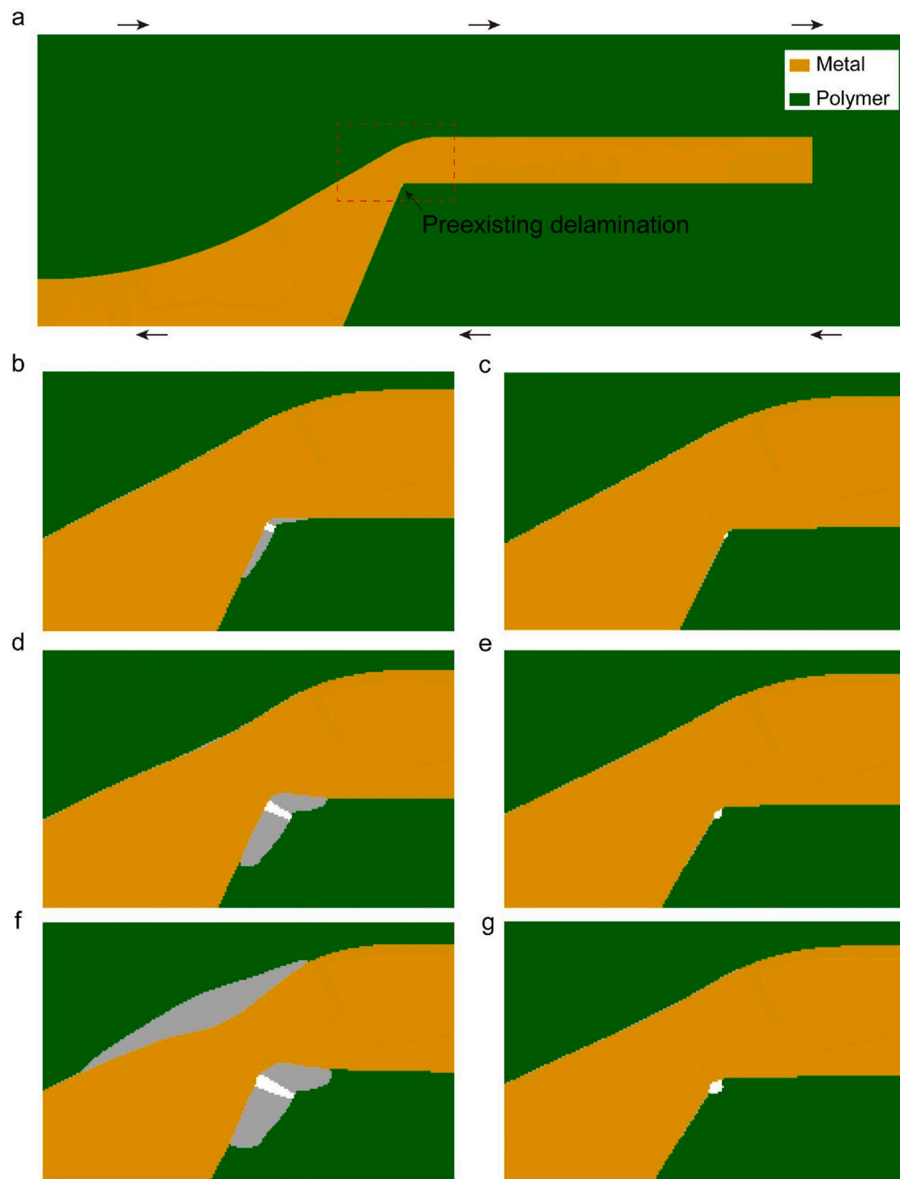

Fig. 6. Simulation of concurrent delamination and deformation. (a) Schematic of part of an integrated structure in which a small preexisting delamination is introduced at the corner of the bottom surface of the metal layer. (b, d, and f) The concurrent deformation and delamination for a weak interface. (c, e, and g) The concurrent deformation and delamination for a strong interface. (b, c) are at a step time of 0.73, (d, e) are at a step time of 0.91 and (f, g) are at a step time of 1.0.

simulation to obtain the delamination observed in the experiment. Because the metal and the polymer deform plastically, the sequence of the applied displacement and change in temperature is significant. We have tried many sequences, and here we describe a particular sequence, which is chosen after many iterations to give the result that necking occurs shortly after the delamination grows. The amplitude of the displacement is programmed to increase cubically with step time, while the temperature decreases linearly with step time. Step time increases from 0 to 1 in the simulation. At the end of the step both temperature and displacement simultaneously reach their final value. Increasing the displacement cubically with step time biases the displacement towards the end of the simulation. By then the decrease in temperature has applied sufficient tensile stress to the interface.

Under stress, the corner at the bottom surface of the metal concentrates stress. When the interface is weak, the initial delamination on the bottom surface of the metal layer gradually grows (Fig. 6b). Once the delamination on the bottom surface extends to become large enough for some deformation to localize, a delamination initiates on the top surface (Fig. 6d). As the delamination on the top surface grows, the presence of delaminations on both surfaces of the metal layer removes the constraint from the polymer, and facilitates further necking of the metal layer (Fig. 6f). The necking grows and, in turn, facilitates the delamination on the top surface of the metal layer. With continued loading, these two concurrent processes–necking and delamination–mutually facilitate each other, ultimately breaking the metal layer (Fig. 1b). By contrast, a strong adhesion between the metal and polymer can suppress the growth of the initial delamination, and thereby suppress deformation localization in the metal layer even at a large strain (Fig. 6c, e, and g).

In addition to adhesion between the metal and the polymer, other variables, such as the radius of curvature at the corner of the metal layer, also affect the concurrent delamination and deformation (Fig. 7). We compare two cases: a corner with a small radius of curvature (Fig. 6a) and a corner with a large radius of curvature (Fig. 7a). In both cases, the same traction-displacement model of weak adhesion is applied. The corner with a small radius of curvature concentrates stress more than the corner with a large radius of curvature. In the former, the concentrated stress causes concurrent delamination and deformation, as described above (Fig. 6b, d, and f). The corner with a large radius of curvature

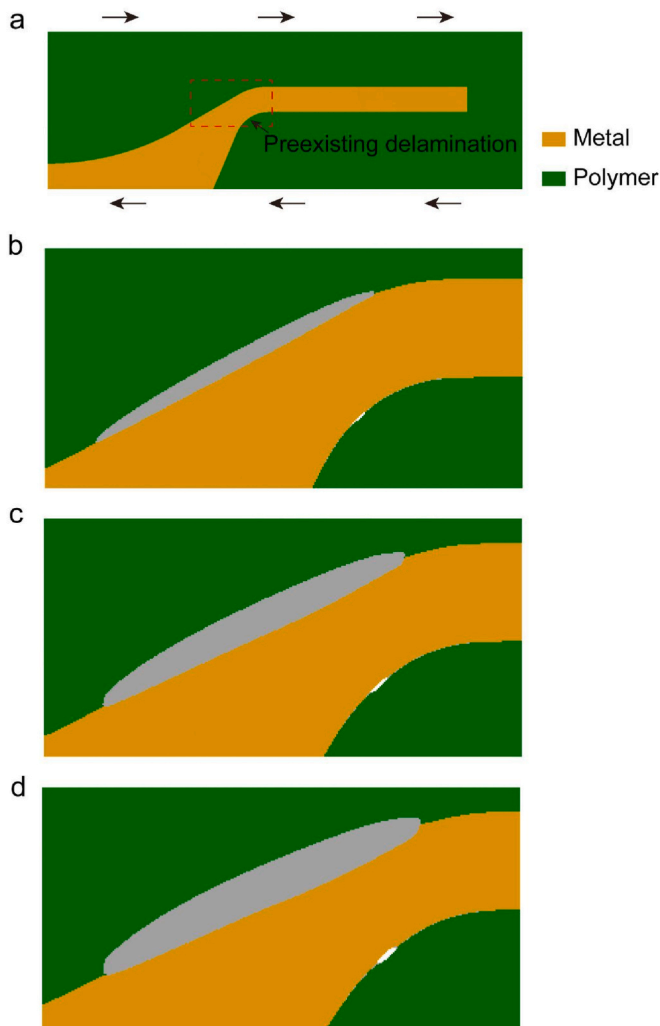

Fig. 7. Effect of corner radius. (a) A corner with a large radius of curvature. The structure at (b) a step time of 0.73, (c) 0.91, and (d) 1.0.

initiates a delamination on the top surface of the metal layer due to thermal expansion mismatch (Fig. 7b). However, because the corner of a large radius of curvature concentrates stress much less than the corner with a small radius of curvature, the preexisting delamination at the corner does not grow (Fig. 7c). The adhesion enables the polymer to constrain the metal, so that the metal does not form a neck (Fig. 7d). A large deformation does not rupture the metal, and therefore does not cause electrical failure.

5. Concluding remarks

We use the finite element method to investigate an experimentally observed failure mechanism in integrated structures of metals and polymers in semiconductor devices: the concurrent propagation of delamination and localization of deformation. Because of the large-scale yielding conditions, linear elastic fracture mechanics does not apply. We model the propagation of delamination using cohesive zone elements. We highlight the delamination between the metal and the polymer as a prerequisite for the necking in the metal. Defects and transverse tensile stress make the structure particularly vulnerable to concurrent delamination and necking. Strong adhesion between the metal and polymer, as well as a large radius of curvature at the corner of the metal layer, can retard the deformation localization, and thereby mitigate the risk of electrical failure. Mechanical and thermal loading both contribute to the failure mechanism. The sequence of the applied displacement and change in temperature is significant, because the metal and the polymer deform plastically. We hope that this study provides insight into failure analysis of integrated structures where large scale yielding and delamination are concurrent. We also hope that this work draws attention from researchers in the field of mechanics and materials to the emerging problems in the development of the semiconductor industry.

CRediT authorship contribution statement

Shawn R. Lavoie: Writing – review & editing, Writing – original draft, Methodology, Investigation, Formal analysis, Conceptualization. **Guodong Nian:** Writing – review & editing, Writing – original draft, Methodology, Formal analysis, Investigation. **Chen-Wei Li:** Investigation. **Jason Lan:** Investigation. **Yu-Sheng Lin:** Investigation. **Yi-Lun Lin:** Investigation. **Sherwin Tang:** Investigation. **Jyun-Lin Wu:** Investigation. **Joost J. Vlassak:** Writing – review & editing, Investigation. **Zhigang Suo:** Writing – review & editing, Writing – original draft, Supervision, Methodology, Funding acquisition, Conceptualization.

Declaration of competing interest

The authors declare no competing interest.

Data availability

Data will be made available on request.

Acknowledgement

The work at Harvard was supported by a contract from TSMC. The paper was submitted to a special issue of Mechanics of Materials in honor of Professor Alan Needleman on the occasion of his eightieth birthday.

References

Barenblatt, G.I., 1959. The formation of equilibrium cracks during brittle fracture. General ideas and hypotheses. Axially-symmetric cracks. J. Appl. Math. Mech. 23, 622–636. https://doi.org/10.1016/0021-8928(59)90157-1.

Dugdale, D.S., 1960. Yielding of steel sheets containing slits. J. Mech. Phys. Solid. 8, 100–104. https://doi.org/10.1016/0022-5096(60)90013-2.

Hui, C.-Y., Jagota, A., Bennison, S.J., Londono, J.D., 2003. Crack blunting and the strength of soft elastic solids. Int. J. Fract. 459, 1489–1516.

Irwin, G.R., 1968. Linear fracture mechanics, fracture transition, and fracture control. Eng. Fract. Mech. 1, 241–257. https://doi.org/10.1016/0013-7944(68)90001-5.

Lau, J.H., 2022. Recent advances and trends in advanced packaging. IEEE Trans. Compon. Packag. Manuf. Technol. 12, 228–252. https://doi.org/10.1109/TCPMT.2022.3144461.

Li, T., Huang, Z., Suo, Z., Lacour, S.P., Wagner, S., 2004. Stretchability of thin metal films on elastomer substrates. Appl. Phys. Lett. 85, 3435–3437. https://doi.org/10.1063/1.1806275.

Li, T., Huang, Z.Y., Xi, Z.C., Lacour, S.P., Wagner, S., Suo, Z., 2005. Delocalizing strain in a thin metal film on a polymer substrate. Mech. Mater. 37, 261–273. https://doi.org/10.1016/j.mechmat.2004.02.002.

Li, T., Suo, Z., 2007. Ductility of thin metal films on polymer substrates modulated by interfacial adhesion. Int. J. Solid Struct. 44, 1696–1705. https://doi.org/10.1016/j.ijsolstr.2006.07.022.

Lu, N., Wang, X., Suo, Z., Vlassak, J., 2009. Failure by simultaneous grain growth, strain localization, and interface debonding in metal films on polymer substrates. J. Mater. Res. 24, 379–385. https://doi.org/10.1557/JMR.2009.0048.

Lu, N., Wang, X., Suo, Z., Vlassak, J., 2007. Metal films on polymer substrates stretched beyond 50. Appl. Phys. Lett. 91, 221909 https://doi.org/10.1063/1.2817234.

Malyshev, B.M., Salganik, R.L., 1965. The strength of adhesive joints using the theory of cracks. Int. J. Fract. Mech. 1, 114–128.

Needleman, A., 1987. A Continuum model for void nucleation by inclusion debonding. J. Appl. Mech. 54, 525–531. https://doi.org/10.1115/1.3173064.

Needleman, A., 1972. A numerical study of necking in circular cylindrical bar. J. Mech. Phys. Solid. 20, 111–127. https://doi.org/10.1016/0022-5096(72)90035-X.

Tvergaard, V., 1990. Analysis of tensile properties for a whisker-reinforced metal-matrix composite. Acta Metall. Mater. 38, 185–194. https://doi.org/10.1016/0956-7151(90)90048-L.

Tvergaard, V., Hutchinson, J.W., 1992. The relation between crack growth resistance and fracture process parameters in elastic-plastic solids. J. Mech. Phys. Solid. 40, 1377–1397. https://doi.org/10.1016/0022-5096(92)90020-3.

Wei, Y., Hutchinson, J.W., 1997. Nonlinear delamination mechanics for thin films. J. Mech. Phys. Solid. 45, 1137–1159. https://doi.org/10.1016/S0022-5096(96)00122-6.

Zhang, T., Yuk, H., Lin, S., Parada, G.A., Zhao, X., 2017. Tough and tunable adhesion of hydrogels: experiments and models. Acta Mech. Sin. 33, 543–554. https://doi.org/10.1007/s10409-017-0661-z.